Sustainable Energy & Fuels

ROYAL SOCIETY OF CHEMISTRY

REVIEW

View Article Online
View Journal | View Issue

Cite this: *Sustainable Energy Fuels*, 2025, **9**, 6586

Computational modelling of metal-supported SOFCs: current approaches and future opportunities

Axel Savikko, Buse Bilbey and Muhammad Imran Asghar *

Metal-supported solid oxide fuel cells (MS-SOFCs) have recently emerged as a promising configuration to reduce material costs and increase the mechanical robustness of solid oxide technologies. Recently, experimental research has focused on addressing fabrication challenges and degradation mechanisms. Computational modelling of MS-SOFCs remains limited, although there are potential benefits to simulation based analysis and optimization. This paper presents the current status of MS-SOFC research, with particular attention to support structures and degradation mechanisms. The paper also presents a foundation for modelling SOFCs at the cell scale, and highlights recent literature that could be adapted for MS-SOFC research. In addition to conventional computational modelling, the potential of data-driven methods such as surrogate models is reviewed for future work. This is the first focused review on computational approaches for MS-SOFCs, providing a foundation for future modelling and optimization of these emerging cell architectures.

Received 28th August 2025
Accepted 1st October 2025

DOI: 10.1039/d5se01161b

rsc.li/sustainable-energy

1 Introduction

The hydrogen economy has recently received a lot of attention as a promising avenue for decarbonisation in several industries.[1] Within the hydrogen sector, solid oxide cells (SOCs) have been shown to be one of the most efficient ways to convert fuel to electricity and *vice versa*. Compared with other fuel cell and electrolyser technologies, other advantages include fuel flexibility, superior performance, and the ability of a cell to run reversibly.[2–4] Fig. 1 shows a schematic of the reversibility of an SOC. Fuel flexibility in fuel cell mode allows the use of other hydrocarbons while producing electricity, whereas in electrolysis mode, it gives the opportunity to directly produce other hydrocarbon-based fuels along with hydrogen.[5] Although SOCs have significant advantages, there are still several challenges to overcome before solid oxide technologies can overtake more conventional alkaline and polymer electrolyte membrane fuel cells and electrolysers.

One major hindrance is the high cost of the materials, making it difficult for SOCs to economically compete with other technologies.[2] Another problem is the degradation levels of the SOCs during operation, as the operating temperature of SOCs is usually 600–1000 °C.[6] High degradation rates reduce the lifespan of the device, which in turn increases the cost of the system because the device must be changed. The target degradation rate for SOCs is 0.2% per 1000 h, but the reported degradation rates remain above 0.5% per 1000 h.[7]

Traditional SOCs consist of three main layers: a fuel electrode, an electrolyte, and an air electrode. To have a mechanically robust cell, one of these layers must act as a support. Practically, this implies that the layer must be thicker than the others. In principle, any layer could act as a support. However, in general, either the electrolyte or the fuel electrode is chosen as the supporting layer.[8] Of these two, the fuel electrode-supported configuration is preferred, as a thick electrolyte significantly decreases the performance of an SOC. The various configurations can be seen in Fig. 2.

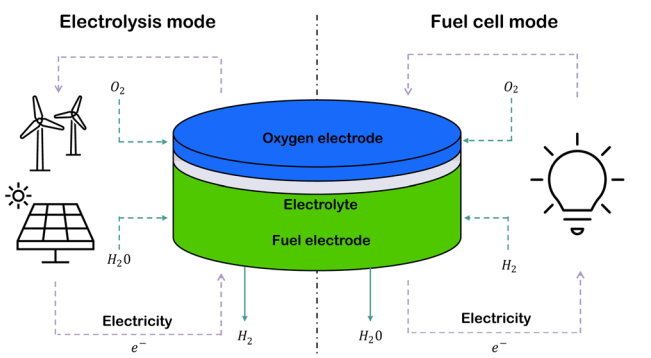

Fig. 1 Schematic of an SOC: SOCs can be operated reversibly, *i.e.* they can be used both in electrolysis mode to produce green hydrogen and in fuel cell mode to generate electricity from hydrogen and other hydrocarbons.

Renewable Energy Technologies Group, Engineering Materials Science, Faculty of Engineering and Natural Sciences, Tampere University, 33720, Tampere, Finland. E-mail: imran.asghar@tuni.fi; Tel: +358 503052503

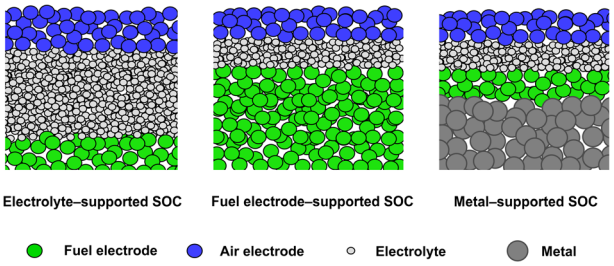

Fig. 2 Various configurations for a single solid oxide cell.

Currently, the trend for SOC research is to reduce operating temperature. For conventional SOCs, the operating temperature can be above 800 °C to achieve sufficient performance. As the cell is exposed to such high temperatures, it poses extensive requirements on the chosen materials to survive such environments. This in turn results in high costs for the system and degradation of the cell components, again increasing the cost over the lifespan of the cell.[9] Reducing the temperature would help bring down the cost of the technology and increase the viability of commercializing the technology.

Another way of decreasing the cost of SOCs is by considering more cost-effective materials. The functional material used in SOC anodes is of high cost. For fuel electrode-supported SOCs, only a fraction of the thickness of the anode facilitates electrochemical reactions. The rest of the anode contributes only by providing mechanical support and electronic conduction. Thus, in recent years, a new configuration has become increasingly popular, where the supporting layer consists of a porous stainless steel substrate, making the so-called metal-supported SOCs (MS-SOCs) as seen in Fig. 2. The stainless steel material used for the metal support is significantly cheaper than the functional material of the anode, reducing the cost of one cell.[10] As an example, ferritic stainless steel grade 316L can be bought from Sandvik AB for 45.46 € per kg, whereas nickel oxide (NiO), a typical anode material, can be bought from FuelCellStore for 545 $ per kg. Additionally for making the cell cheaper to manufacture, the metal support provides other improvements as well, along with new challenges. These will be discussed in more detail in Section 2.

The majority of on-going research on MS-SOCs is experimental. Many of the problems are related to the fabrication of the cells, making experimental studies naturally more viable than computational studies. However, as the research develops, there are more and more possibilities of using computational research for MS-SOCs. Utilizing computational research could reduce material waste and increase time-efficiency, accelerating the research of MS-SOCs. This review paper looks into what the current trend is in experimental research of MS-SOCs, what methods are being used in modelling conventional SOCs on the cell level, and how existing computational methods could be utilized for research on metal-supported SOCs.

1.1 Working principle

SOCs operate by utilizing a solid oxide electrolyte to conduct ions at high temperatures, enabling the conversion of chemical energy into electrical energy in fuel cell mode, and *vice versa* in electrolysis mode. SOCs can be broadly classified into solid oxide fuel cells (SOFCs) and solid oxide electrolysis cells (SOECs), each with distinct operating principles and applications.

The materials in SOCs are, as the name suggests, solid oxide materials. The three main parts of an SOC, the electrolyte and the fuel and air electrodes, all have specific requirements for the chosen material. The electrolyte needs to conduct ions, while being electronically insulating. The two most common electrolyte materials are yttria-stabilized zirconia (YSZ) and gadolinium-doped ceria (GDC),[11] whereas other materials such as barium zirconium cerium yttrium ytterbium (BZCYYb) materials have recently been researched.[12] For the electrodes, the main desired properties are high catalytic activity for their respective reactions and high electrical conductivity. For the fuel electrode, the most common material is nickel oxide (NiO), while the air electrode often uses perovskite type materials such as lanthanum manganite strontium (LSM) and lanthanum strontium cobalt ferrite (LSCF).[13]

The choice of the electrolyte material divides both SOFCs and SOECs into two more categories, depending on which ion the electrolyte conducts. The two types are oxygen-ion conducting and proton-conducting, which can be abbreviated as O-SOC and H-SOC. Proton-conducting solid oxide cells are sometimes referred to as protonic ceramic cells in the literature. The working principles of all categories are similar, with small differences based on which mode the cell is operated in and what electrolyte the cell has.

1.1.1 Solid oxide fuel cells. In fuel cell mode, a fuel such as hydrogen is supplied to the fuel electrode and air is supplied to the air electrode. The gases then diffuse through the porous electrodes to reach the interface between the electrodes and the electrolyte. The boundary where the gas phase, electrode phase and electrolyte phase meet is called the triple phase boundary (TPB). The TPB is where the electrochemical reactions of an SOFC occur.

The electrochemical reactions differ depending on the type of SOFC. For an O-SOFC, the oxygen molecules in the air electrode are reduced to ions according to eqn (1). The oxygen-ions that are produced are conducted through the electrolyte and react with the hydrogen molecules at the fuel electrode side to produce water according to eqn (2).

$$\frac{1}{2}O_2 + 2e^- \rightarrow O^{2-} \quad (1)$$

$$H_2 + \frac{1}{2}O_2 \rightarrow H_2O \quad (2)$$

In H-SOFCs, the hydrogen molecules are oxidized at the fuel electrode according to eqn (3). The protons are then conducted through the electrolyte, where they react with the oxygen molecules creating water according to eqn (4).

$$H_2 \rightarrow 2H^+ + 2e^- \quad (3)$$

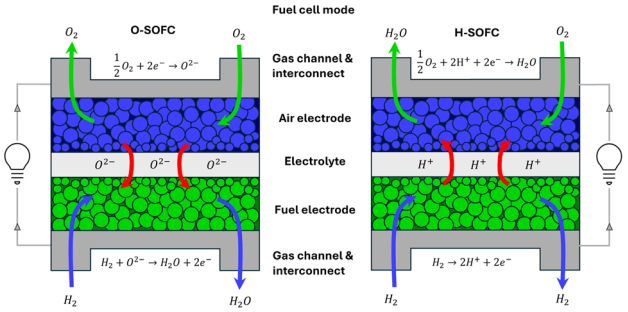

Fig. 3 Working principle for O-SOFCs and H-SOFCs.

$$\frac{1}{2}O_2 + 2H^+ \rightarrow H_2O \quad (4)$$

By connecting the electrodes through an external circuit, a current can be drawn from the configuration. The schematic of the working principle for O-SOFCs and H-SOFCs can be seen in Fig. 3.

1.1.2 Solid oxide electrolysis cells. SOECs are very similar to their fuel cell counterparts in terms of the working principle. In the case of water electrolysis, the gas that is supplied to the cell is water vapor. The electrode to where the vapor is supplied depends on the choice of electrolyte. For O-SOECs, the water vapor is supplied to the fuel electrode and for H-SOECs to the air electrode.

In O-SOECs, the water vapor is split into hydrogen and oxygen ions at the interface between the electrolyte and fuel electrode due to the current applied to the cell. The reaction can be seen in eqn (5). The oxygen ion then travels through the electrolyte and is reduced to oxygen gas according to eqn (6), which is then pumped out of the cell. The hydrogen is produced at the fuel electrode, where it is pumped out with the unreacted water vapor. Fig. 4 displays the working principle for both O-SOECs and H-SOECs.

$$H_2O + 2e^- \rightarrow 2H^+ + O^{2-} \quad (5)$$

$$O^{2-} \rightarrow \frac{1}{2}O_2 + 2e^- \quad (6)$$

For H-SOECs, the water vapor reacts at the interface between the air electrode and the electrolyte, producing oxygen gas and hydrogen ions. The hydrogen ions then travel through the electrolyte to the fuel electrode, where it is oxidized into pure hydrogen gas.

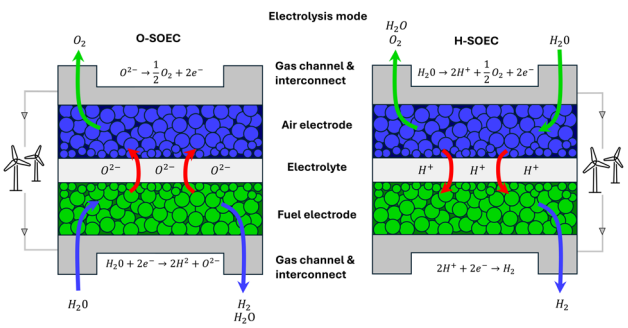

Fig. 4 Working principle for O-SOECs and H-SOECs.

Although both SOFCs and SOECs have been considered so far in this review, the analysis will now continue by focusing on SOFCs, as the majority of metal-supported studies are on fuel cells. Many of the considerations in this paper can be extended to electrolysis cells as well.

2 Metal-supported solid oxide fuel cells

Metal-supported solid oxide fuel cells (MS-SOFCs) employ a support layer made of metal instead of the conventional ceramic material. Compared to a traditional ceramic support layer made out of an anode material, the metal support gives many benefits. The main attraction is the reduced cost of the material by changing a large portion of the expensive ceramic material to a cheaper stainless steel alternative.[14–16] Metal-supported variants also have better thermal properties due to the increased thermal conductivities of stainless steel. This results in better resistance to thermal shocks and tolerance to thermal cycling.[16–18] An added bonus of the metal material is the possibility of sealing the cell through conventional means such as welding. This eliminates the need for other expensive sealants and simplifies the building of stacks.[19] The metal support also provides superior mechanical robustness compared to the traditional material. These traits are desirable for SOFCs, as it reduces the risk of mechanical failure.[20,21]

There are several requirements for a metal support for it to be suitable for use in SOFCs. First, as the layer is supposed to provide support, it needs sufficient mechanical strength.[22] Furthermore, the metal support should have sufficient porosity for mass transport, sufficient electronic conduction for low ohmic losses, and chemical stability with the anode layer to avoid side reactions.[23] Metal supports also need thermal coefficients compatible with the anode layer to avoid thermal stresses.[24]

Over the past decade, several studies have been conducted on metal-supported SOFCs (MS-SOFCs). Many of these studies have been included in some of the review papers that have been published *e.g.* by Tucker *et al.*[14] and Krishnan *et al.*[10] This section presents a brief review of current experimental research on MS-SOFCs, summarizing the state-of-the-art and other relevant research questions that have been answered.

2.1 State of the art

Some of the highest-performing MS-SOFCs are presented in Table 1. Performances are generally reported for a temperature range of 600–800 °C and various environments with varying hydrogen contents, which influences the achieved maximum power density. Thus, these are also included in the table. The material choices seem pretty typical for both the fuel electrode, *i.e.* the anode in fuel cell mode, and the electrolyte, with nickel dominating the choice for anode material and both YSZ and doped ceria being the typical choice for the electrolyte.

Table 1 The highest performing MS-SOFCs

Metal	Anode|electrolyte|cathode	Environment	Temperature (°C)	Power density (W cm^{-2})	References
Fe26Cr, ITM	Ni-YSZ/Ni-GDC|YSZ|LSC	50% H_2 50% H_2O	800	3.13	25
P434L	Ni-SDC|SCSZ|Pr_6O_{11}	Humified H_2	700	1.5	26
Ni-10w.% Fe alloy	Ni-GDC|GDC|LSCF-GDC	Wet H_2	700	1.278	27
Cr-based STS	NiO-GDC|ScYSZ|LSC-GDC	80–96% H_2 4–20% H_2O	650	1.14	28
Hastelloy X	NiO-SDC|SDC|SSCo	97% H_2 3% H_2O	650	0.75	29

However, the choice for the air electrode, *i.e.* the cathode material is more varied.

To the best of our knowledge, the highest performing MS-SOFC is reported by Udomslip *et al.* in the cell concept of Plansee SE. The high performance is mainly attributed to the optimized microstructure of the highly active Ni-GDC anode and $La_{0.58}Sr_{0.4}CoO_{3-\delta}$ (LSC) cathode, along with the thin 2 μm YSZ electrolyte. At 800 °C, the cell has a power density of 3.13 W cm^{-2}, whereas at 650 °C, the power density is 1.96 W cm^{-2}, even outperforming conventional anode-supported SOFCs. The highlight of this research is that the high performance was achieved without the use of novel and complex materials, but with careful optimization and fundamental understanding of the device.[25] Dogdibegovic *et al.* also produced a high performing MS-SOFC, but their key approach included the use of infiltrated electrodes. The infiltration method allows for better control on the microstructure of the electrodes, resulting in a high active area. At the same time, this results in high degradation rates. The use of a highly active Pr_6O_{11} cathode material also contributed to the high performance.[26] To decrease degradation rates, the microstructure was altered, reducing the maximum power point by 35%, but achieving stable operation for 200 h.[26]

2.2 Metal support structures

There are different variants of the metal supports in terms of the structure itself, as shown in Fig. 5. Most of the structures are so-called porous metal supports, where the gases diffuse through the pores of the substrate. Hui *et al.* demonstrated this structure by using a commercially available SS430 porous substrate.[30] Instead of using commercial substrates, porous substrates can be fabricated in house. Toor and Croiset fabricated a simple porous metal substrate using the pressing method, which is suitable for laboratory-scale fabrication.[31] Zhou *et al.* produced metal substrates made of Fe30Cr using tape casting.[32] Dogdibegovic *et al.* used P434 stainless steel powder to fabricate a porous metal support for both the anode and cathode sides using tape casting as seen in Fig. 5a.[26,33]

Instead of using a porous substrate, some studies employed metal supports based on stainless steel sheets or foil. To introduce the mass flow channels to the support layer, Ceres power used laser drilling to periodically drill holes into the foil, which facilitates the mass transfer of fuel from the gas channels to the anode. Fig. 5d show the structure of the Ceres power cell, containing (1) the metal support, (2) the laser-drilled holes, (3) the fuel electrode, (4) the electrolyte, (5) the active air electrode and (6) the air electrode diffusion layer.[34] Similarly, Lee *et al.* used a 0.2 mm thick Crofer22APU stainless steel sheet, where they used chemical etching to make periodic holes with a diameter of 0.2 mm as seen in Fig. 5c.[35] In another research group, Lee and Bae employed a different geometry for the mass flow channels in the support layer. They used a sheet of STS430 stainless steel, where a zigzag-shaped hole seen in Fig. 5b was cut using the wire cutting method.[36] The difference between this strategy and the two previous ones is that here there is only one long hole, instead of many small holes.

There are certain strengths and weaknesses between the powder-based and sheet-based substrates. The powder-based substrates are easier to manufacture, as techniques used for ceramic processing (*e.g.* tape casting) can be used to manufacture metal substrates. In contrast, laser-drilled sheets have an advantage against oxidation, as the exposed surface area is much smaller than that of powder-based substrates. However, the cost of producing these substrates is higher than that of powders, as drilling the gas diffusion holes requires high-cost laser equipment. The chemically etched substrates have the same strengths as the laser-drilled substrates. However, as only one paper has reported using such a substrate without describing the process extensively, it is difficult to evaluate its suitability for commercial production.

2.3 Degradation

The commercial use of MS-SOFCs requires long operating lifetimes with limited degradation. The introduction of a stainless

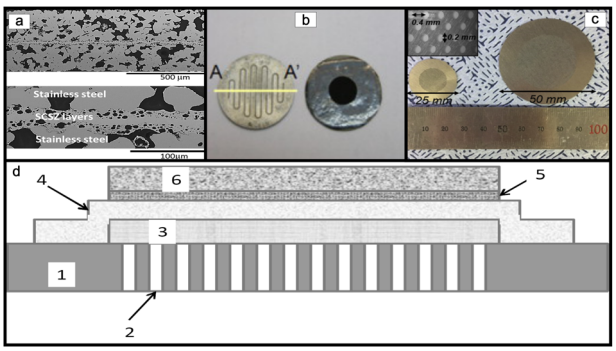

Fig. 5 Selection of various metal support types from the literature. (a) Cross section of a symmetric porous metal support. Reprinted with permission from Elsevier.[26] (b) Wirecut zigzag pattern in a metal sheet. Reprinted with permission from Elsevier.[36] (c) Chemically etched holes in a metal sheet. Reprinted with permission from Elsevier.[35] (d) Schematic of a Ceres' power MS-SOFC with drilled holes in a metal sheet. Reprinted with permission from IOP publishing Ltd.[34]

steel material in the support layer introduces new types of degradation that need to be taken into account when designing the cell. The main types of degradation are oxidation of the metal substrate, delamination between the metal support and ceramic anode, and inter-diffusion of elements between the two layers. This section presents the main types of degradation for MS-SOFCs.

2.3.1 Oxidation of metal supports. A key difference between conventional and metal supports is the oxidation susceptibility of the metal support. At the high temperatures of typical SOFC operating conditions (600–800 °C), the commonly used ferritic stainless steel materials can form oxide scales when exposed to oxygen or water vapor. These scales can decrease electrical conductivity and mechanical robustness, effectively decreasing the lifetime of the metal support. Understanding and limiting the extent of metal support oxidation is key to extending its lifetime.[37,38]

During fabrication, the metal layer is exposed to temperatures up to 1350 °C. Due to the high temperature, this process is done under reducing conditions.[39] Fu *et al.* investigated the oxidation behavior of the metal substrate during the fabrication of an MS-SOFC. They found that even though sintering is done under reducing conditions, there might still be trace amounts of oxygen that lead to significant oxidation during the fabrication process. Oxidation during fabrication can alter the porosity of the metal substrate, lowering its mass transport properties. To mitigate oxidation, the researchers used an oxygen-adsorbent agent of titanium, as well as mixing up to 10% YSZ in the metal support to create gas channels.[40]

The long-term durability of metal supports is highly dependent on the oxidation of the metal support during operation at high temperatures. Xu *et al.* performed a long-term test, in which they exposed a 430L stainless steel metal support to dry air at 800 °C for 1500 h. The aim was to understand the oxidation behavior of the metal substrate, as it would be used for scaffolding in a symmetric cell, where the metal would also be exposed to air during operation. The researchers showed that the substrate exhibited a weight gain of 3 wt%. Although the effect on performance is not quantified, the weight gain from the chromium scale indicates lowered electronic conduction and mechanical integrity.[41] Xu *et al.* also conducted a similar study, using the same parameters except for the fact that they used a reducing atmosphere instead of an oxidizing atmosphere. The results show similarities with those of the oxidizing case. The weight gain was also observed to be 3 wt% in the reducing atmosphere due to the presence of water vapor. The predicted lifetime of the substrate was 10 000 h.[42]

2.3.2 Inter-diffusion. Nickel is one of the most commonly used materials for SOFC anodes, also in the context of MS-SOFCs. When nickel is in contact with the chromium-rich stainless steel of the metal support during cell operation, inter-diffusion of nickel into the metal support and chromium and iron into the anode occurs. When nickel enters the metal support, it can form an austenitic grade of steel, which in turn induces a mismatch in the coefficient of thermal expansion, leading to thermal stresses. The chromium and iron that is diffusing into the anode can cause scale formation on the active nickel, reducing the TPB length, *i.e.* reducing the performance of the anode. The interdiffusion can be reduced by introducing a diffusion barrier layer between the anode and the metal support, consisting of *e.g.* GDC.[43] Brandner *et al.* used a CeO_2 barrier layer between a FeCr metal substrate and NiO anode. A cell without a barrier layer was fabricated for comparison. The cell with a barrier layer showed a much smaller concentration of chromium in the anode, and exhibited a power density of 430 mW cm^{-2}, whereas the cell without a barrier layer could not produce any measurable power.[44] Similarly, Kim *et al.* used a $Y_{0.08}Sr_{0.88}TiO_3$–YSZ diffusion barrier layer, which successfully prevents interdiffusion. However, the cell presents poor performance, but according to the researchers it is not caused by the diffusion barrier layer.[45]

2.4 Thermal effects

It is important for the metal support and the ceramic layer attached to the metal support to have matching coefficients of thermal expansion (CTE), as the cell undergoes high temperature variations during fabrication and start-up. A mismatch in the CTE will induce stress, which ultimately could lead to delamination between the anode and metal support.[38,46]

By comparing the CTE between typical material choices for metal supports and anodes or electrolytes, suitable pairs can be chosen. The commonly used ferritic stainless steels have a CTE of 11.5–14 $\times$ 10^6 K^{-1}, whereas typical ceramic components of SOFCs have a CTE of 10–13 $\times$ 10^6 K^{-1}. Although there is no significant difference in the CTE of the materials, even a small difference can cause large stresses due to the high operating temperature of SOFCs.[38]

As outlined in this section, MS-SOFCs offer advantages such as lower cost and improved robustness, but they also introduce new challenges related to oxidation, thermal stress, and degradation at material interfaces. Many of these issues are difficult to study experimentally, particularly during long-term operation. In this regard, modelling becomes a valuable tool for understanding key processes, supporting design optimization, and identifying potential failure modes. The following section outlines modelling approaches used in SOFC research and how they can support MS-SOFC development.

3 Review of modelling techniques and topics for SOFCs

Modelling of SOFCs can be done at multiple scales, from the microscale of electrochemical reactions using density functional theory (DFT) to large-scale system modelling.[47] The effect of the metal support is mainly noticed on a single cell or stack scale, which is why the focus of this paper is on unit cell scale modelling.

The modelling of MS-SOFCs is very similar to modelling conventional SOFCs. The only thing that differs between the two configurations is the support layer. The support layer itself contributes to the general performance of an SOFC through mass flow, heat transfer, and electronic conduction; thus, evaluating the performance of the metal support would require

only modelling of these properties. However, it might be difficult to compare MS-SOFCs with other configurations solely on the basis of the support layer. By modelling the whole MS-SOFC, the performance of the support can be quantified from the performance of the whole cell. This section presents a basis of equations upon which a single cell MS-SOFC can be modelled. This is mostly based on SOFC models, as they are in essence the same. The section will also present all available literature on MS-SOFC numerical modelling, along with conventional SOFC numerical modelling that has potential for use in MS-SOFC modelling.

Modelling an SOFC is inherently a multiphysical problem. There are three main types of physics needed to fully model an SOFC – electrochemical properties, thermal properties, and flow of different types in different parts.[48] Table 2 shows the various required physics for the different parts of an SOFC.

For a single cell simulation, the flow of gases is at the core. Thus, it is natural to use computational fluid dynamics (CFD) as a basis for SOFC simulation. Coupling the gas flow to electrochemical reactions and heat transfer makes for a complete modelling package. Such coupled modelling is called multiphysics modelling. Software such as COMSOL Multiphysics, Ansys Fluent and OpenFOAM are well suited for these kinds of problems.[49,50]

3.1 Governing equations

Governing equations are the core of computational modelling of SOFCs. The governing equations are required to mathematically describe the working principle of an SOFC discussed in the introduction. This section introduces a general set of governing equations, which can be solved using the typical software mentioned before.

3.1.1 Voltage. The reversible fuel cell voltage, also known as open circuit voltage E^{OCV}, is defined as the difference in the thermodynamic potentials of the electrode reactions. The open circuit voltage also depends on the operating conditions of the system. The Nernst equation describes the E^{OCV} of a H_2–O_2 fuel cell for any temperature and pressure based on eqn (7).[51]

Table 2 Summary of the required physics for modelling each SOFC part

Sofc part	Required physics
Porous electrode	Flow in porous media
	Electrochemical reactions
	Electronic conduction
	Ionic conduction
	Thermal effects
Electrolyte	Ionic conduction
	Thermal effects (electronic conduction)
Support	Flow in porous media
	Electronic conduction
	Thermal effects
Interconnect	Electronic conduction
	Thermal effects
Gas channels	Flow in free media
	Thermal effects

$$E^{OCV} = E^0 - \frac{RT}{2F}\ln\left(\frac{pH_2O}{pH_2pO_2^{0.5}}\right) \quad (7)$$

The open-circuit voltage only applies at zero current. Once the current is drawn, the voltage decreases due to three different overpotentials seen in eqn (8).[51]

$$E = E^{OCV} - \eta_{act} - \eta_{ohm} - \eta_{conc} \quad (8)$$

The concentration overpotential η_{conc} is associated with the mass transfer of reactants to the reaction sites as defined in eqn (11). The ohmic overpotential η_{ohm} is related to conduction mechanisms and their resistance according to eqn (10). The activation overpotential η_{act} is defined in eqn (9), where Φ_s stands for the electric potential and Φ_l is the ionic potential. The activation overpotential depends on the reaction rate at the electrodes, where fast reactions result in a low activation overpotential and *vice versa*.[52]

$$\eta_{act} = \Phi_s - \Phi_l - E^{OCV} \quad (9)$$

$$\eta_{ohm} = \frac{il_E}{\sigma_E} \quad (10)$$

$$\eta_{conc} = \frac{RT}{2F}\ln\left(\frac{pH_2}{pH_{2,TPB}}\frac{pH_2O_{TPB}}{pH_2O}\right) + \frac{RT}{4F}\ln\left(\frac{pO_2}{pO_{2,TPB}}\right) \quad (11)$$

The current produced by an SOFC is determined by electrochemical reactions. Electrochemical reactions occur in the porous electrodes. The reactions in turn are dependent on the reaction kinetics of the system. There are a couple of ways to model the reaction kinetics of an SOFC; however, the Butler–Volmer formulation is most widely used. The equation for local current density i_{loc} based on the Butler–Volmer formulation is shown in eqn (12).[53,54]

$$i_{loc} = i_0\left(e^{\frac{\alpha n_e F}{RT}\eta_{act}} - e^{\frac{-(1-\alpha)n_e F}{RT}\eta_{act}}\right) \quad (12)$$

Here, i_0 is the exchange current density, α is the transfer coefficient, n_e is the number of electrons transferred in the reaction, F is Faraday's constant, R is the gas constant, T is the temperature, and η_{act} is the activation overpotential. The transfer coefficient is usually assumed to be 0.5. The exchange current density can be determined through the semi-empirical formulae in eqn (13) and (14), for anodes and cathodes, respectively.[54]

$$i_{0,an} = \gamma_{an}\left(pH_{2,an}\right)^a\left(pH_2O_{an}\right)^b e^{-\frac{E_{act,an}}{RT}} \quad (13)$$

$$i_{0,cat} = \gamma_{cat}\left(pO_{2,cat}\right)^m e^{-\frac{E_{act,cat}}{RT}} \quad (14)$$

The equations include the partial pressures of both the reactants and the products, as well as several empirical parameters; the prefactor γ, activation energy E_{act}, and the

exponents a, b, and m. The empirical parameters need to be identified *via* experiments. In eqn (13) and (14), it is assumed that the reacting species are hydrogen and oxygen.

3.1.2 Mass transport. As the electrochemical reactions occur at the TPB, near the electrode–electrolyte interphase, the reactants need to travel from the gas channels through the porous electrodes to the reaction sites. This transport is diffusive in nature. The mass transport is governed by the equation for the species conservation seen in eqn (15).[55]

$$\frac{\partial}{\partial t}(\rho\omega_i) + \nabla\cdot(\rho\omega_i u) = -\nabla\cdot j_i + R_i \quad (15)$$

In eqn (15), ω_i is the weight fraction of species i, ρ is the density of the mixture, u is the mass average velocity of the mixture, R_i is the rate of the source term and j_i is the mass flux. The mass flux is described by diffusion models. The typical choices for the diffusion models include Fick's law model (FL), the Maxwell–Stefan model (MS) and the dusty gas model (DG). The MS model is typically preferred, due to a higher precision than FL, with reasonable computational cost.[55–57] By substituting the mass flux given by the MS model, the transport equation for the species conservation becomes

$$\rho\frac{\partial}{\partial t}(\omega_i) + \rho(u\cdot\nabla)\omega_i = \nabla\left(\rho\omega_i\sum_k D_{ik}\mathbf{d}_k + {D_i}^T\frac{\nabla T}{T}\right) + R_i \quad (16)$$

$$\mathbf{d}_k = \nabla x_k + \frac{1}{p_\mathrm{A}}[(x_k - \omega_k)\nabla p_\mathrm{A}] \quad (17)$$

In eqn (16) and (17), D_{ik} is the multi component Maxwell–Stefan diffusivity, Di^T is the thermal diffusion coefficient x_k is the mole fraction of species k and T is temperature. The diffusional driving force $\mathbf{d}_k$ is defined in eqn (17). The multi component Maxwell–Stefan diffusivity coefficients are determined using the Fuller–Schettler–Giddings (FGS) approach according to eqn (18).[58]

$$D_{ij} = 1.01325\cdot10^{-2}T^{1.75}\frac{\left(\frac{1}{M_i}+\frac{1}{M_j}\right)^{0.5}}{p\left(v_i^{1/3}+v_j^{1/3}\right)^2} \quad (18)$$

Since SOFC electrodes are porous, effective diffusivity must be calculated to account for reduced transport pathways. This is often done using the Bruggeman correction in eqn (19), which modifies the bulk diffusion coefficient based on porosity ε.

$$D_{ij,\mathrm{eff}} = \varepsilon^{1.5}D_{ij} \quad (19)$$

3.1.3 Momentum transfer. The velocity and pressure of the relevant gases are solved through momentum transfer using the Navier–Stokes equations in the free flow regions, as shown in eqn (20), along with the conservation of mass as shown in eqn (21). In porous regions, the drag effect of porosity and permeability is added to the Navier–Stokes equations resulting in the so-called Brinkman equations as shown in eqn (22) and the corresponding conservation of mass as shown in eqn (23).[55,59]

$$\rho\frac{\partial u}{\partial t} + \rho(\mathbf{u}\cdot\nabla)\mathbf{u} = \nabla\left[-p\mathbf{I} + \mu\left(\left(\nabla\mathbf{u} + (\nabla\mathbf{u})^T\right) - \frac{2}{3}(\nabla\cdot\mathbf{u})\mathbf{I}\right]\right] + \mathbf{F} \quad (20)$$

$$\frac{\partial\rho}{\partial t} + \nabla\cdot(\rho\mathbf{u}) = 0 \quad (21)$$

Here, $\mathbf{u}$ stands for velocity, p for pressure, $\mathbf{I}$ is the identity matrix, T is the absolute temperature, $\mathbf{F}$ is the volume force vector and μ is the dynamic viscosity of the gas.

$$\frac{\rho}{\varepsilon}\left[\frac{\partial u}{\partial t} + (\mathbf{u}\cdot\nabla)\frac{\mathbf{u}}{\varepsilon}\right] = \nabla\left[-p\mathbf{I} + \mu\left(\left(\nabla\mathbf{u} + (\nabla\mathbf{u})^T\right) - \frac{2}{3}(\nabla\cdot\mathbf{u})\mathbf{I}\right]\right] - \left(\mu k^{-1} + \frac{Q_\mathrm{m}}{\varepsilon^2}\right)\mathbf{u} + \mathbf{F} \quad (22)$$

$$\frac{\partial}{\partial t}(\varepsilon\rho) + \nabla\cdot\rho\mathbf{u} = Q_m \quad (23)$$

Here, ε stands for porosity and k for permeability, both of which are parameters of the porous region. Q_m stands for a mass source or sink in the porous region.

3.1.4 Heat transfer. An accurate temperature distribution within an SOFC is important for accurate modelling results, as many processes in the SOFC are temperature dependent. SOFCs typically involve all types of heat transfer, *i.e.* conduction, convection and radiation, due to their high operating temperature.[60,61] There are two main ways of modelling heat transfer in SOFCs, the local temperature equilibrium (LTE) method and the local temperature non-equilibrium (LTNE) method. In LTE, the temperature of the gas and solid phase is assumed to be locally the same, whereas in LTNE that is not the case. The temperature between the gas and the solid phase has been found to not vary significantly. This enables the successful use of LTE instead of LTNE, providing a great reduction in computational demand.[62,63]

The temperature distribution in an SOFC is solved through the heat balance equation in eqn (24) when using the LTE approach.[55,64]

$$\rho C_\mathrm{p}\frac{\partial T}{\partial t} + \rho C_\mathrm{p}\ \mathbf{u}\cdot\nabla T = \nabla\left(k_\mathrm{eff}\nabla T\right) + Q \quad (24)$$

Here, C_p is the specific heat capacity, ρ is the density, $\mathbf{u}$ is the velocity of the gas, k_eff is the effective thermal conductivity and Q is the source term. The thermal conductivity is effective because it includes the effects of both the gas and solid through eqn (25), where k_g is the gas phase thermal conductivity and k_s is the solid phase thermal conductivity.

$$k_\mathrm{eff} = \varepsilon_\mathrm{p}\cdot k_\mathrm{g} + (1 - \varepsilon_\mathrm{p})\cdot k_\mathrm{s} \quad (25)$$

By coupling these equations, an SOFC model encompassing mass, momentum, charge and heat transfer with electrochemical reactions can be built. However, to successfully utilize numerical methods, simplifications are necessary to reduce computational complexity. Boundary conditions and initial

values also need to match with the given problem. The following subsection lists the most commonly used assumptions and boundary conditions.

3.1.5 Modelling assumptions and boundary conditions. The mathematical model of an SOFC relies on several assumptions to simplify the complex physical and chemical phenomena. To retain a sufficient accuracy in the models balanced with reasonable computational cost, the following assumptions are commonly made:[65,66]

- Steady-state operation is assumed unless otherwise specified.
- Ideal gas behavior is assumed for all gaseous species.
- The porous electrodes are isotropic and homogeneous, with constant porosity and permeability.
- Thermophysical and electrochemical properties (*e.g.*, conductivity, diffusivity, and exchange current density) are either constant or follow temperature-dependent empirical relations.
- The Local Thermal Equilibrium (LTE) assumption is applied, meaning the gas and solid phases share the same temperature.
- Radiation heat transfer is neglected due to its relatively minor effect compared to conduction and convection.

Boundary conditions are defined based on the physical layout of the cell. Commonly applied boundary conditions include:

- Gas channels: known inlet temperature, composition, and flow rate; outlet typically set to reference pressure.
- Solid walls: no-slip velocity boundary condition for gas flow; insulated or symmetric boundary for heat transfer.
- Electrodes: applied current density or cell voltage specified at the external circuit.
- Electrolyte: zero electronic conductivity and ionic potential continuity across interfaces.

With the full set of equations, boundary conditions and assumptions, the basis for an SOFC model is complete.

3.2 Literature on modelling studies

While Section 3.1 outlined the fundamental governing equations used for SOFC modelling on the cell scale, this section reviews existing numerical studies relevant to MS-SOFCs. Although the majority of MS-SOFC research to date has been experimental, some computational studies have recently begun emerging. This section first reviews the limited number of studies that directly simulate MS-SOFCs, followed by a wide overview of work on conventional SOFCs that could be adapted to the metal-supported configuration.

3.2.1 Numerical modelling studies specific to MS-SOFCs. To date, only a limited number of numerical studies on MS-SOFCs have been reported. Park *et al.* developed a three-dimensional model of an MS-SOFC to compare it against an anode-supported SOFC. The model included the conservation of mass, momentum, energy and species, coupled to electrochemical reactions. The study showed that the MS-SOFC performed worse than the conventional SOFC. However, the modelled MS-SOFC employed a 2 mm thick metal support, which is thicker than a typical metal support.[67] Zhang *et al.* also developed a three-dimensional model for an MS-SOFC using a ceria based electrolyte. The model was similar to that of Park *et al.*, but also included a detailed radiation heat transport model. It was found that the radiation heat flux accounts for 3.16% of the total heat flux. The study shows that an MS-SOFC yields a more uniform temperature distribution, but the metal support has a negative influence on the mass transport of reactants.[68]

Wang *et al.* developed a two-dimensional model for a tubular SOFC, which they used to compare an anode supported configuration against a metal supported one. The model included the same conservation equations as the three-dimensional models, but additionally the study included direct internal reforming and thermal stresses. The study found that due to the superior thermal conductivity of the metal support, the thermal stresses were smaller in the MS-SOFC, which ultimately resulted in a lower failure rate. The work was continued in another paper from 2021.[69,70]

Leah *et al.* developed an electrochemical model based on the Ceres power MS-SOFC, which has a drilled metal support instead of a porous one. The model only includes a simple one dimensional diffusion model for mass transfer instead of a comprehensive CFD model. On top of the 1D cell model, the study includes a stack level and system level study using the MS-SOFC. Although the simple 1D model gives insight on how the gases diffuse from the holes to the porous electrode, the behavior of the full cell should be analyzed with a comprehensive cell scale model.[71]

To highlight the lack of numerical research on MS-SOFCs, a literature sweep was conducted on Google Scholar. Using the search query "x supported solid oxide fuel cell numerical model", where x stands for an anode, electrolyte or metal, the first ten pages were analyzed and the amount of relevant papers from 2005–2025 were recorded. The results of the search are seen in Fig. 6. Throughout the period, the amount of anode supported papers remains dominant, whereas the other support types can be found in lower amounts. In terms of anode-supported papers, this graph does not encompass all of the available literature, whereas all the available MS-SOFC numerical studies known to the author are included.

3.2.2 Cell design and geometry optimization through modelling. Modelling of SOFCs has been used to investigate a broad range of topics. The main benefit of fast and inexpensive study setups makes modelling an excellent tool for optimization. In terms of SOFCs, optimization can be in terms of *e.g.* cell design, material choice and operating conditions. Optimizing cell design through experiments would lead to fabrication of tens or hundreds of cells, whereas utilizing modelling could highlight the best possibilities, which could then be validated through experiments. This approach reduces both the cost of materials used, and the amount of time spent on the optimization problem.

Optimization of SOFC design through modelling has been shown in the literature. In terms of cell design, mass transport is an important factor for SOFC performance. Andersson *et al.* investigated the optimal gas channel geometry of a single SOFC

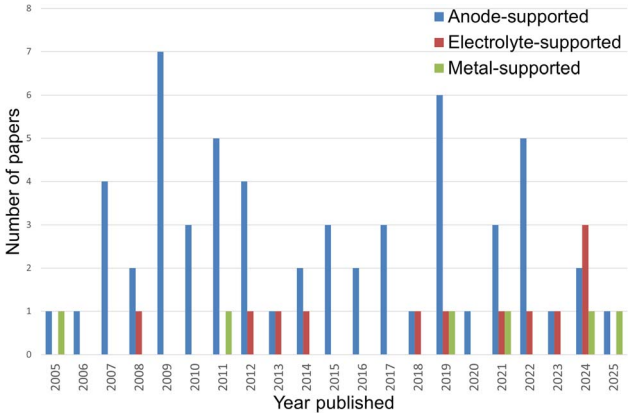

Fig. 6 Number of published numerical studies on anode-supported, electrolyte-supported and metal-supported SOFCs from 2005–2025. Produced *via* a literature sweep on Google Scholar.

based on a computational fluid dynamics approach and managed to increase the volumetric power density while only decreasing the cell current density by a small amount.[72] Khazaee *et al.* compared three different geometries for the gas channels of an SOFC, rectangular, triangular and trapezoidal, and found that the rectangular geometry provided the best performance.[73]

Due to the conventional structure of the interconnects, parts of the cell are not in direct contact with the supplied gases. This makes the design of the interconnects an important aspect of how gases diffuse under the interconnect rib. To investigate the optimal design, Guo *et al.* designed an SOFC model to study the effect of the interconnect design on the performance of the cell. The study found that an increase of 27.86% can be achieved by optimizing the design.[74] Fu *et al.* investigated a novel design called the beam and slot interconnector, which was shown to eliminate the limitation of gas diffusion based on the interconnect ribs.[75]

3.2.3 Thermal analysis and stress modelling. Beyond performance optimization, modelling plays a key role in understanding degradation and failure mechanisms. In particular, thermal gradients can induce significant stress within the cell, potentially leading to cracking or delamination. Since local temperatures are difficult to measure experimentally, simulations offer a crucial tool for visualising temperature distributions and designing more thermally stable cells.

Atif Mahmood *et al.* coupled a typical multiphysics model of an SOFC with equations for thermal stress and strain. Using the model, the effect of various factors such as operating parameters, flow configurations and material properties on the thermal stress of the cell was studied.[76] Wu *et al.* investigated a novel flow field configuration, and its effect on the maximum thermal gradient. It was shown that by optimizing the flow field, the maximum gradient dropped by 50.86%.[77]

Thermal cycling is generally an issue for the lifetime of an SOFC. Liu *et al.* developed a thermomechanical model for an SOFC to calculate thermal stresses and predict crack growth under thermal cycling conditions. Although the model is not coupled to other physics, the model efficiently described critical failures of SOFCs.[78]

3.2.4 Transient modelling. Transient modelling of SOFCs is essential for capturing the dynamic behavior of SOFCs under real-word operating conditions. Unlike steady-state models, transient models account for time-dependent phenomena such as load changes, startup and shutdown sequences, and thermal cycling.[79]

Modelling of startup sequences is important for SOFCs due to their high operating temperatures. Reaching the desired temperature efficiently without introducing large thermal gradients is important for a safe startup. Kupecki *et al.* investigated a novel startup sequence *via* 3D CFD modelling, where fuel used in the SOFC is also used for heating up the cell. The results of the modelling show a shortened start-up time, with a high level of temperature uniformity.[80] Zhu *et al.* also investigated transient thermal stress behavior of a conventional SOFC during start-up using CFD combined with computational structural mechanics (CSD). By comparing conventional rectangular interconnects to cylindrical interconnects, it was found that the latter result in reduced thermal stress during start-up.[81]

Beyond thermal management, load regulation is crucial for real-world operation of SOFCs. Li *et al.* considered a dynamic 3D CFD model of an SOFC to investigate how step changes in the inlet gas temperature, inlet gas flow rate and output voltage affect power density. The results showed a two-stage response with the fast response driven by changes in reactant concentrations and the slow response caused by changes in cell temperature. Four control schemes were tested to regulate the power density by ±20%.[82] Similarly, Zhu *et al.* investigated the dynamic response of an SOFC operated on syngas instead of hydrogen through a 2D single-channel model. It was shown that after a change in flow rate, the SOFC stabilizes in approximately 100 seconds.[83]

3.2.5 Internal reforming. The high operating conditions of SOFCs combined with their catalytic activity also allow them to use other hydrocarbons as fuel through internal reforming. The main alternative fuel is methane, but other fuels such as ethanol, methanol and biogas have also been studied. Numerical simulations have been increasingly used to help design and optimize direct internal reforming SOFCs (DIR-SOFCs).[84]

The study by Ma *et al.* presents a validated 3D multiphysics model for DIR-SOFCs fueled by a mixture of hydrogen and natural gas. The results of the study show that the DIR-SOFC stack has large thermal gradients due to competing endothermic and exothermic reactions. It was also shown that by operating at thermal-neutral voltage the thermal stress can be lowered.[85]

3.2.6 Degradation and lifetime prediction modelling. Numerical modelling can be very beneficial for degradation and lifetime prediction. To be produced experimentally, these results need experiments spanning thousands of hours. With modelling, SOFC operation can be simulated for thousands of hours in a fraction of that time. Thus, it is highly useful to guide such experiments through numerical modelling, as has been shown previously.

Babaie Rizvandi *et al.* developed a multiscale 3D model of a full SOFC stack, incorporating three degradation mechanisms: nickel particle coarsening, chromium poisoning and metallic interconnect oxidation. A total of 38 thousand hours of operation was simulated, allowing the researchers to find optimum operating conditions.[86] Naeini *et al.* developed a mathematical model for degradation of SOFCs. The model can predict the effect of nickel coarsening and oxidation, anode pore size changes and other relevant degradation mechanisms. The model shows that current density has the highest effect on degradation rates, whereas H_2 partial pressure has the least effect.[87]

Lifetime prediction models are typically made with experimental data. Khan *et al.* conducted a long-term performance test on a short SOFC stack by performing electrochemical impedance spectroscopy (EIS) every 200 hours to monitor the degradation. Based on the results, a mathematical model was developed, which estimated the lifetime of the stack to be over 50 000 h.[88]

3.3 Machine learning approaches in SOFC modelling

Machine learning (ML) refers to data-driven techniques that infer input–output relationships from data, often without relying on explicit physical models. These approaches have gained traction in electrochemical systems, including SOFCs, where they are applied to tasks such as performance prediction and microstructure analysis. Compared with the multiphysics modelling techniques described earlier, ML has a much lower computational cost. This is because ML models do not incorporate real physics equations like multiphysics modelling does. Instead, ML models learn the relationship between inputs and outputs solely based on data. However, this limits the models to devices or topics for which there exists sufficient data. As long as the data are of good quality and in large quantities, ML models make for efficient and relatively accurate models for certain topics. Due to their computational efficiency, ML models are particularly useful for optimization and rapid design screening. Table 3 shows a comparison of typical neural network architectures discussed in this section.

3.3.1 Performance prediction from experimental data. The use of experimental data for ML is a powerful way of interpreting and using the data, as long as it is of good quality and in sufficient amounts. Golbabaei *et al.* compared various ML methods for predicting the voltage of an anode-supported SOFC based on 6 input variables. The methods included linear regressors, *K*-nearest neighbors, neural networks and others. It was found that an artificial neural network (ANN) with a multilayer perceptron (MLP) architecture provided the best accuracy in predicting the voltage. The training data consisted of 403 experimental observations from another author.[89] Subotic *et al.* used a novel approach of combining experimental data and data from a multiphysics simulation. Several hundreds of such data points were used to train an ANN that was used to predict both the polarization curve and impedance of the cell based on temperature, current density and fuel composition. The ANN was shown to agree well with the measured data.[90]

3.3.2 Surrogate modelling. Surrogate modelling replaces conventional multiphysics simulations with faster, data-driven approximations. Typically, simulation data are first generated across a range of input conditions. A machine learning model is then trained to emulate the simulation outputs, enabling rapid prediction without re-running the full physical model. The strengths of surrogate modelling is that data can be made as much as is needed, but the data is limited to what a multiphysics simulation can produce.

Surrogate modelling can already be found in SOFC modelling literature. Xu *et al.* utilized surrogate modelling based on an ANN with a structure seen in Fig. 7a combined with the genetic algorithm (GA) based on a CFD model of a single SOFC to optimize its performance based on 10 input parameters. The author was able to increase the power density of the SOFC by 109.6% compared to the base simulation by utilizing GA and the surrogate model.[91] Xing *et al.* developed a multi-fidelity surrogate modelling framework for SOFC optimization using a Bayesian feature-enhanced stochastic collocation method. Their approach enables accurate, high-resolution predictions of spatially distributed quantities without requiring low-fidelity outputs at inference time. By incorporating engineered features, the model efficiently replaces full 3D CFD simulations and supports multi-objective optimization with significantly reduced computational cost.[92]

3.3.3 Microstructure evolution and performance modelling using machine learning. Machine learning (ML) is increasingly being applied to study the evolution of microstructures in SOFC materials, offering a powerful alternative to traditional phase-field or empirical models. These approaches aim to predict how features such as pore networks, grain boundaries, or phase distributions change during processes like reduction, oxidation, or long-term operation. Many types of convolutional neural networks (CNNs) are utilized for this purpose, as they are well suited for treating images and grid-like data.[93]

Table 3 Advantages and disadvantages of typical neural network structures used for SOFC applications

Neural network	Advantages	Disadvantages
ANN	Easy to implement and train Suitable for surrogate modelling and parameter estimation	Requires a large amount of data Does not exploit spatial data May overfit without regularization
CNN	Excellent for spatial data Useful for 2D or 3D modelling of SOFCs	Higher computational cost due to longer training times Requires large training datasets
PINN	Incorporates governing equations into training Works well with limited data	Training can be difficult and slow Still emerging

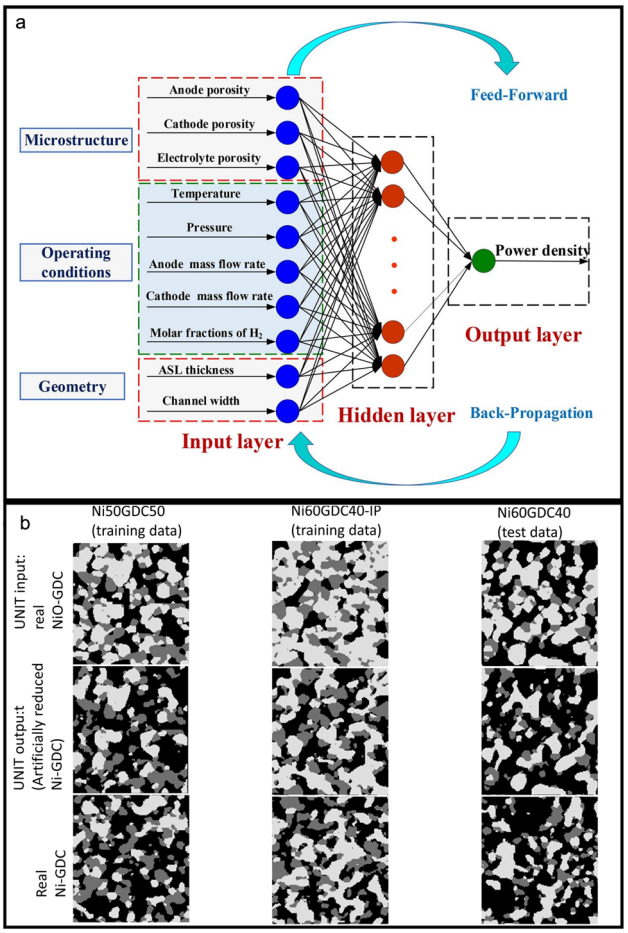

Fig. 7 Machine learning efforts in SOFC research. (a) The neural network structure used by Xu *et al.*[91] Reprinted with permission from Elsevier. (b) Comparison of real and predicted Ni-GDC microstructures.[94]

Sciazko *et al.* investigated the use of a conditional unsupervised image-to-image translation network (C-UNIT) in predicting the reduction process of Ni-YSZ and Ni-GDC based anodes. The network was trained on unpaired images of Ni-YSZ and Ni-GDC microstructures before and after reduction. The results showed an excellent agreement between the predicted microstructure and the actual imaged microstructure, as seen in Fig. 7b. The C-UNIT was even able to successfully predict microstructures that were not part of the training set.[94]

Yan *et al.* developed a method of optimizing the microstructure of an SOFC cathode from fabrication to operation using an ANN. The ANN is trained on cathode overpotentials that have been calculated using the Lattice Boltzmann Method (LBM) on synthetic cathodes. A total of 770 numerical simulations were used as training data. The model is able to predict degradation rates and cathodic overpotentials based on initial powder characteristics. By coupling the model to GA, optimized initial conditions for the powders were obtained.[95]

3.3.4 Physics informed neural networks. An emerging class of machine learning models, known as physics-informed neural networks (PINNs), has gained attention for modelling complex physical systems where data may be limited or expensive to generate. Unlike conventional neural networks trained solely on data, PINNs incorporate the governing physical laws—typically expressed as partial differential equations—directly into the loss function during training.[96]

Although PINNs have not been used to simulate single SOFCs, many studies have been reported that could be used for SOFCs. Berardi *et al.* developed a PINN for modelling transport in porous materials, such as diffusion, which is highly applicable for SOFCs.[97] Laubscher developed a PINN capable of predicting momentum, species and temperature distribution of a dry air humidification problem.[98] Studies like these could help in extending the use of PINNs for SOFCs, by incorporating electrochemical reactions and other components required by SOFCs.

4 Translating computational methods to MS-SOFC challenges

As discussed previously, MS-SOFC research remains mostly experimental. Although some modelling papers can be found for MS-SOFCs, many research topics remain unexplored. This section will highlight what kind of modelling techniques could be adapted from conventional SOFC research to answer MS-SOFC specific research questions. Fig. 8 shows various research directions for future numerical studies on MS-SOFCs.

4.1 Adapting multiphysics modelling to MS-SOFCs

The difference between conventional SOFCs and MS-SOFCs lies in the support layer. As the difference is fairly minimal, many multiphysics models could be directly adapted for MS-SOFCs. The required changes are related to the specific design of MS-SOFCs and the parameters of the specific microstructure. The material-specific parameters also need to be properly defined, including, *e.g.* electrical conductivity and thermal conductivity. Such a model would be able to predict the performance of an MS-SOFC fairly well, although without the effect of degradation. Unfortunately, many experimental papers on MS-SOFCs lack important parameters, such as porosity or CTE, which would allow for a direct recreation of such a cell computationally. This results in computational researchers either having to fabricate their own cells with which they could build and validate an MS-SOFC model, or search for relevant parameters in other papers.

Successfully incorporating degradation mechanisms into multiphysics models for MS-SOFCs would be a valuable asset in optimizing both geometries and operating conditions for MS-SOFCs. A similar approach as that of Rizvandi *et al.*[86] could be used. The degradation mechanisms that are most vital to consider would be the oxidation of the metal support and the thermal stress between the metal support and the ceramic anode. In this way, the support and operating conditions could easily be tailored to minimize both degradation, which in turn maximizes the lifetime of the cell. The effect of oxidation of the metal support on the porosity and the mass transport properties of MS-SOFCs would also be an interesting topic. To pursue this,

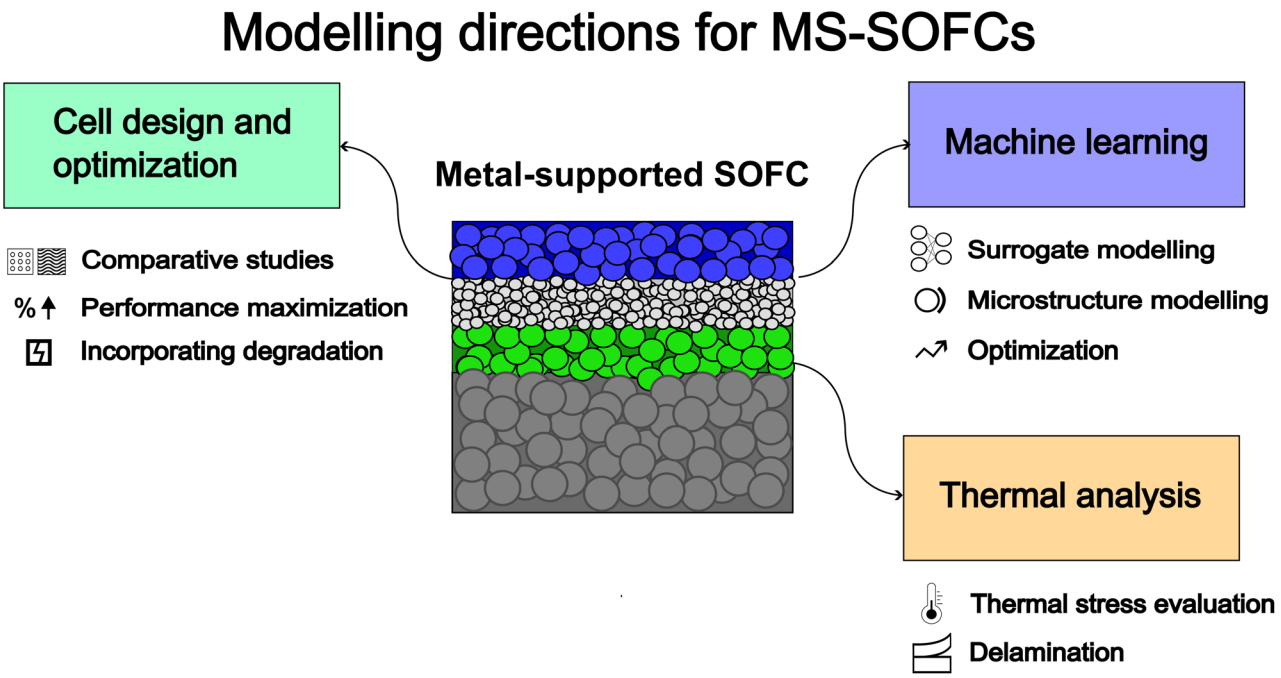

Fig. 8 Various modelling directions for future MS-SOFC numerical studies.

a well-established and validated multiphysics model for MS-SOFCs should exist, which is currently not the case.

4.2 Cell and geometry optimization for MS-SOFCs

Cell and geometry optimization is one of the most promising modelling applications for MS-SOFCs. The use of metal supports enables diverse gas flow configurations, which can be systematically explored through simulations. For example, modelling can be used to determine the optimal number, size, and distribution of gas diffusion holes in sheet-based metal supports.

To compare how the different support configurations affect the device performance might be difficult from individual experimental studies. There are a lot of parameters in all the studies in terms of the fully fabricated device. The studies might employ different materials for the SOFC part, different fabrication strategies, and different geometries and parameters. All these aspects influence the performance of the MS-SOFC, which usually is the target of these studies. Given the differences in the studies, it might be difficult to quantify the benefits of the chosen metal support type. Utilizing modelling, the functional part of the SOFC can be kept constant while changing the metal support configuration.

Optimization of an MS-SOFC using a porous substrate would not differ very much from modelling conventional SOFCs aside from parameters, but modelling a laser-drilled MS-SOFC could prove to be difficult. The holes in the stainless steel sheet are very small and abundant, which could increase the difficulty of reaching convergence in its simulation. Modelling the gas flow in the narrow holes requires intricate meshing, which can increase the computational load, specifically for large scale 3D simulations. Instead of modelling them directly, the holes could also be treated as effective porosity, but such a drastic simplification could hide important details, such as what kind of thermal stresses a laser-drilled substrate endures.

Aside from already mentioned metal structures, modelling could essentially be used to generate whole new support configurations that have not been reported in experimental research. The freedom of producing a digital geometry could yield a higher performing support configuration than what is currently known. However, although the performance might be better, it does not ensure that the configuration is viable to produce experimentally. This highlights the need for experimental validation, as the strengths of modelling cannot be utilized unless there is a real physical outcome of it.

4.3 Using machine learning for MS-SOFCs

Machine learning presents an interesting option for MS-SOFC modelling. MS-SOFCs are going to gain a lot from optimization, which is a task specially suited for ML. Making surrogate models of MS-SOFCs using multiphysics models could accelerate the optimization of the metal supports. The surrogate models could be used to optimize the supports in terms of gas transport, degradation rates, or both, depending on how the model is made. Complex support structures could also stand to gain from the strengths of PINNs. In the future, ML will increasingly be used in conjunction with multiphysics models, as software starts including methods to generate surrogate models within multiphysics software.

Beyond surrogate models, machine learning can also be applied to microstructural analysis in MS-SOFCs. Inspired by the work of Sciazko *et al.*, ML models could be trained to predict the oxidation behavior on the basis of the material properties and initial microstructure of the metal support. Although there

are some models for the oxidation of metal supports in the literature, an ML model could predict oxidation as seen from experiments. The ML model could most likely also be connected to a multiphysics model, making the multiphysics model closer to a real simulation.

The limiting factor for efficient use of machine learning in MS-SOFC research is the lack of publicly available data. Machine learning needs a large amount of good quality data, while the novelty of MS-SOFCs makes such data scarce. Any researcher that wants to utilize machine learning for their research has to generate their data themselves, making the workload larger than for other topics.

4.4 Bridging experiments and modelling in MS-SOFCs

Currently, most experimental MS-SOFC studies do not include modelling of any kind. At the same time, MS-SOFC modelling studies include only slight validation against experimental data, if any. In the future, it could be beneficial to have tighter integration between the two research methods. Modelling could be used to design experimental work by narrowing down parameter ranges or choosing an initial optimal geometry to fabricate. This way, the expensive and time consuming experiments are conducted optimally, but the models are still true to reality as the results are recreated experimentally.

To facilitate ML research for MS-SOFCs, it would be of great benefit to crowd-source data. This would require researchers to keep their data open-source, while clearly labeling it. The amount of good quality data is key to increasing the accuracy of ML models. By collaborating in the effort of data generation, the community would together accelerate future research on MS-SOFCs.

There is a strong opportunity to lead the future of MS-SOFC development with computational means. More importantly, the collaboration between experimental and modelling research will be key for low-cost, reliant, and well performing MS-SOFCs.

5 Conclusions

Metal-supported SOFCs offer clear advantages compared to conventional SOFCs, including lower cost, mechanical robustness and better thermal cycling. Research into MS-SOFCs is relatively novel, with most work being experimental. In this paper, the prospects of using modelling to advance MS-SOFC research were evaluated.

The state of the art for MS-SOFCs was summarized from the literature, whereas current modelling efforts for general SOFC research were also covered. Using this as a foundation, the key opportunities for utilizing modelling techniques on the cell scale for MS-SOFC research were identified. The paper focused on multiphysics modelling, while novel machine learning methods were also covered.

MS-SOFCs aim to benefit from modelling studies, particularly for optimizing tasks and understanding degradation mechanisms. From analyzing thermal stresses of specific cell structures to investigating the influence of oxidation on mass transport properties of the substrate, there are many opportunities to utilize modelling. The fast and inexpensive methods can cover large parameter sets quickly compared to experiments, which can be utilized to guide experimental research and cell design.

As metal-supported SOFCs move toward commercial viability, computational modelling will play an increasingly important role in guiding their design, understanding degradation, and accelerating optimization. Bridging the current gap between experimental and computational efforts will be essential to unlock the full potential of MS-SOFC technology.

Author contributions

Axel Savikko: conceptualization, formal analysis, investigation, methodology, visualization, writing – original draft, writing – review and editing. Buse Bilbey: investigation, writing – review and editing. Muhammad Imran Asghar: conceptualization, formal analysis, investigation, methodology, project administration, supervision, visualization, writing – review and editing.

Conflicts of interest

There are no conflicts to declare.

Data availability

No primary research results, software or code have been included and no new data were generated or analysed as part of this review.

Acknowledgements

The authors are thankful to the Research Council of Finland (Grant No. 13322738 and 31213593551), Business Finland (Grant No. 1846/31/2023), and Tampere University through the Tenure Start Grant for tenure-track professors (Grant No. 12967928) for the financial support.

Notes and references

1 J. Yap and B. McLellan, *Int. J. Hydrogen Energy*, 2024, **66**, 371–386.
2 M. Singh, D. Zappa and E. Comini, *Int. J. Hydrogen Energy*, 2021, **46**, 27643–27674.
3 S. Y. Gómez and D. Hotza, *Renewable Sustainable Energy Rev.*, 2016, **61**, 155–174.
4 M. B. Mogensen, M. Chen, H. L. Frandsen, C. Graves, J. B. Hansen, K. V. Hansen, A. Hauch, T. Jacobsen, S. H. Jensen, T. L. Skafte and X. Sun, *Clean Energy*, 2019, **3**, 175–201.
5 C. Graves, S. D. Ebbesen, S. H. Jensen, S. B. Simonsen and M. B. Mogensen, *Nat. Mater.*, 2015, **14**, 239–244.
6 H. Yokokawa, H. Tu, B. Iwanschitz and A. Mai, *J. Power Sources*, 2008, **182**, 400–412.
7 S. Zarabi Golkhatmi, M. I. Asghar and P. D. Lund, *Renewable Sustainable Energy Rev.*, 2022, **161**, 112339.
8 N. Q. Minh, *Solid State Ionics*, 2004, **174**, 271–277.

9 E. D. Wachsman and K. T. Lee, *Science*, 2011, **334**, 935–939.
10 V. V. Krishnan, *WIREs Energy Environ.*, 2017, **6**, e246.
11 P. Vinchhi, M. Khandla, K. Chaudhary and R. Pati, *Inorg. Chem. Commun.*, 2023, **152**, 110724.
12 S. Guo, L. Jiang, Y. Li, P. Zhong, S. A. Ismail, T. Norby and D. Han, *Adv. Funct. Mater.*, 2024, **34**, 2304729.
13 F. S. da Silva and T. M. de Souza, *Int. J. Hydrogen Energy*, 2017, **42**, 26020–26036.
14 M. C. Tucker, *J. Power Sources*, 2010, **195**, 4570–4582.
15 P. Blennow, T. Klemenso, A. Persson, K. Brodersen, A. K. Srivastava, B. R. Sudireddy, S. Ramousse and M. Mogensen, *ECS Trans.*, 2011, **35**, 683.
16 S. Opakhai and K. Kuterbekov, *Energies*, 2023, **16**, 4700.
17 H. Xu, Y. Han, J. Zhu, M. Ni and Z. Yao, *Energy Rev.*, 2024, **3**, 100051.
18 Y. Zhou, J. Li, H. Nie, S. Wang and Z. Zhan, *Kuei Suan Jen Hsueh Pao/Journal of the Chinese Ceramic Society*, 2013, **41**, 936–943.
19 S.-W. Baek, J. Jeong, S. Lee and J. Bae, *ECS Trans.*, 2009, **25**, 2909.
20 A. Hagen, X. Sun, B. R. Sudireddy and H. Persson, *J. Electrochem. Soc.*, 2020, **167**, 104510.
21 Y. M. Park, J. H. Kim and H. Kim, *Int. J. Hydrogen Energy*, 2012, **37**, 555–565.
22 F. Capotondo, M. T. Bishop, F. Palmerini, A. L. Smitshuysen, S. Pirou, B. R. Sudireddy and A. Hagen, *J. Power Sources*, 2024, **613**, 234812.
23 D. Al-Kattan, P. Lenormand, F. Mauvy and P. Rozier, *Fuel Cells*, 2018, **18**, 18–26.
24 Y. Yan, R. Bateni, J. Harris and O. Kesler, *Surf. Coat. Technol.*, 2015, **272**, 415–427.
25 D. Udomsilp, J. Rechberger, R. Neubauer, C. Bischof, F. Thaler, W. Schafbauer, N. H. Menzler, L. G. J. d. Haart, A. Nenning, A. K. Opitz, O. Guillon and M. Bram, *Cell Rep. Phys. Sci.*, 2020, **1**, 1–11.
26 E. Dogdibegovic, R. Wang, G. Y. Lau and M. C. Tucker, *J. Power Sources*, 2019, **410–411**, 91–98.
27 Q. Li, X. Wang, L. Jia, B. Chi, J. Pu and J. Li, *Mater. Today Energy*, 2020, **17**, 100473.
28 T. Klemensø, J. Nielsen, P. Blennow, A. Persson, T. Stegk, B. Christensen and S. Sønderby, *J. Power Sources*, 2011, **196**, 9459–9466.
29 R. Hui, J. O. Berghaus, C. Decès-Petit, W. Qu, S. Yick, J.-G. Legoux and C. Moreau, *J. Power Sources*, 2009, **191**, 371–376.
30 S. R. Hui, D. Yang, Z. Wang, S. Yick, C. Decès-Petit, W. Qu, A. Tuck, R. Maric and D. Ghosh, *J. Power Sources*, 2007, **167**, 336–339.
31 S. Y. Toor and E. Croiset, *ECS Trans.*, 2017, **78**, 2051.
32 Y. Zhou, X. Ye, J. Li, Z. Zhan and S. Wang, *J. Electrochem. Soc.*, 2014, **161**, F332.
33 E. Dogdibegovic, F. Shen, R. Wang, I. Robinson, G. Y. Lau and M. C. Tucker, *ECS Trans.*, 2019, **91**, 877.
34 R. T. Leah, A. Bone, A. Selcuk, D. Corcoran, M. Lankin, Z. Dehaney-Steven, M. Selby and P. Whalen, *ECS Trans.*, 2011, **35**, 351.
35 K. Lee, J. Kang, J. Lee, S. Lee and J. Bae, *Int. J. Hydrogen Energy*, 2018, **43**, 3786–3796.
36 C. Lee and J. Bae, *J. Power Sources*, 2008, **176**, 62–69.
37 M. Reisert, V. Berova, A. Aphale, P. Singh and M. C. Tucker, *Int. J. Hydrogen Energy*, 2020, **45**, 30882–30897.
38 P. Du, J. Wu, Z. Li, X. Wang and L. Jia, *Materials*, 2023, **16**, 3978.
39 M. C. Tucker, G. Y. Lau, C. P. Jacobson, L. C. DeJonghe and S. J. Visco, *J. Power Sources*, 2007, **171**, 477–482.
40 S. Fu, J. Zhang, K. Xu, J. Yang and L. Zhu, *Front. Energy Res.*, 2023, **11**, year.
41 K. Xu and L. Zhu, *Metals*, 2024, **14**, 475.
42 K. Xu, Z. Chen, C. Bao, W. Yan, W. Tang, K. Xu, W. Guan, G. Li, Y. Chen and L. Zhu, *Int. J. Hydrogen Energy*, 2024, **73**, 577–589.
43 P. Satardekar, V. M. Sglavo and D. Montinaro, *Int. J. Appl. Ceram. Technol.*, 2015, **12**, E61–E67.
44 M. Brandner, M. Bram, J. Froitzheim, H. P. Buchkremer and D. Stöver, *Solid State Ionics*, 2008, **179**, 1501–1504.
45 K. J. Kim, S. J. Kim and G. M. Choi, *ECS Trans.*, 2013, **57**, 897.
46 R. P. Reolon, S. Sanna, Y. Xu, I. Lee, C. P. Bergmann, N. Pryds and V. Esposito, *J. Mater. Chem. A*, 2018, **6**, 7887–7896.
47 K. N. Grew and W. K. S. Chiu, *J. Power Sources*, 2012, **199**, 1–13.
48 S. Kakaç, A. Pramuanjaroenkij and X. Y. Zhou, *Int. J. Hydrogen Energy*, 2007, **32**, 761–786.
49 B. Ghorbani and K. Vijayaraghavan, *Int. J. Hydrogen Energy*, 2019, **44**, 13700–13727.
50 openFuelCell2: A new computational tool for fuel cells, electrolyzers, and other electrochemical devices and processes – ScienceDirect, **https://www.sciencedirect.com/science/article/pii/S0010465524000158**.
51 Y. Patcharavorachot, A. Arpornwichanop and A. Chuachuensuk, *J. Power Sources*, 2008, **177**, 254–261.
52 S. Yang, T. Chen, Y. Wang, Z. Peng and W. G. Wang, *Int. J. Electrochem. Sci.*, 2013, **8**, 2330–2344.
53 S. A. Hajimolana, M. A. Hussain, W. M. A. W. Daud, M. Soroush and A. Shamiri, *Renewable Sustainable Energy Rev.*, 2011, **15**, 1893–1917.
54 A. Leonide, Y. Apel and E. Ivers-Tiffee, *ECS Trans.*, 2009, **19**, 81.
55 Z. Zhou, L. Xing, V. Venkatesan, H. Xu, W. Chen and J. Xuan, *Fuel Cells*, 2023, **23**, 119–134.
56 I. K. Iliev, A. R. Gizzatullin, A. A. Filimonova, N. D. Chichirova and I. H. Beloev, *Energies*, 2023, **16**, 7265.
57 S. N. Ranasinghe and P. H. Middleton, *2017 IEEE International Conference on Environment and Electrical Engineering and 2017 IEEE Industrial and Commercial Power Systems Europe*, EEEIC/I&CPS Europe, 2017, pp. 1–6.
58 E. N. Fuller, P. D. Schettler and J. C. Giddings, *Ind. Eng. Chem.*, 1966, **58**, 18–27.
59 J. Hussain, R. Ali, M. N. Akhtar, M. H. Jaffery, I. Shakir and R. Raza, *Curr. Appl. Phys.*, 2020, **20**, 660–672.
60 W. Cai, J. Yuan, Q. Zheng, W. Yu, Z. Yin, Z. Zhang, Y. Pei and S. Li, *Crystals*, 2022, **12**, 1697.
61 D. Sánchez, A. Muñoz and T. Sánchez, *J. Power Sources*, 2007, **169**, 25–34.

62 D. L. Damm and A. G. Fedorov, *J. Power Sources*, 2006, **159**, 1153–1157.
63 Z. He, E. Birgersson and H. Li, *Energy*, 2014, **70**, 478–492.
64 M. Andersson, H. Paradis, J. Yuan and B. Sundén, *Electrochim. Acta*, 2013, **109**, 881–893.
65 N. A. M. N. Aman, A. Mcuhtar, M. R. Somalu, M. I. Rosli, N. A. Baharuddin and N. S. Kalib, *Int. J. Integr. Eng.*, 2018, **10**, 87–92.
66 F. Zabihian and A. S. Fung, *J. Renewable Sustainable Energy*, 2017, **9**, 054301.
67 J. Park, Y.-M. Kim and J. Bae, *Int. J. Hydrogen Energy*, 2011, **36**, 3167–3178.
68 M. Zhang, E. Wang, M. Ni, K. Zheng, M. Ouyang, H. Hu, H. Wang, L. Lu, D. Ren and Y. Chen, *Heliyon*, 2024, **10**, year.
69 Y. Wang, J. Ren, Y. Shi and X. Li, *ECS Trans.*, 2019, **91**, 2013.
70 J. Ren, W. Yuqing and Y. Shi, *Int. J. Green Energy*, 2022, **19**, 399–409.
71 R. T. Leah, N. P. Brandon and P. Aguiar, *J. Power Sources*, 2005, **145**, 336–352.
72 M. Andersson, J. Yuan and B. Sundén, *Fuel Cells*, 2014, **14**, 177–188.
73 I. Khazaee and A. Rava, *Energy*, 2017, **119**, 235–244.
74 M. Guo, Q. He, C. Cheng, D. Zhao and M. Ni, *J. Power Sources*, 2022, **533**, 231373.
75 Q. Fu, Z. Li, W. Wei, F. Liu, X. Xu and Z. Liu, *Energy Convers. Manage.*, 2021, **241**, 114277.
76 M. Atif Mahmood, T. Nawaz Chaudhary, M. Farooq, M. Salman Habib, A. O. M. Maka, M. Usman, M. Sultan, S. Shiung Lam and B. Chen, *Sustain. Energy Technol. Assess.*, 2023, **57**, 103241.
77 J. Wu, J. Hu, Z. Tu and R. Hu, *Int. J. Hydrogen Energy*, 2025, **135**, 339–350.
78 L. Liu, G.-Y. Kim and A. Chandra, *J. Power Sources*, 2010, **195**, 2310–2318.
79 D. Bhattacharyya and R. Rengaswamy, *Ind. Eng. Chem. Res.*, 2009, **48**, 6068–6086.
80 J. Kupecki, D. Mich and K. Motylinski, *Pol. J. Chem. Technol.*, 2017, **19**, 67–73.
81 Y. Zhu, J. Wang, Y. Sun, C. Hong, C. Xu, S. Serbin and D. Chen, *Int. Commun. Heat Mass Transfer*, 2025, **160**, 108391.
82 B. Li, C. Wang, M. Liu, J. Fan and J. Yan, *Renewable Energy*, 2023, **218**, 119266.
83 P. Zhu, Z. Wu, Y. Yang, H. Wang, R. Li, F. Yang and Z. Zhang, *Appl. Energy*, 2023, **349**, 121655.
84 H. H. Faheem, S. Z. Abbas, A. N. Tabish, L. Fan and F. Maqbool, *J. Power Sources*, 2022, **520**, 230857.
85 Q. Ma, X. Zhang, H. Fang, B. Zhu, Y. Wu and X. Xu, *J. Power Sources*, 2025, **631**, 236226.
86 O. Babaie Rizvandi, X.-Y. Miao and H. L. Frandsen, *Int. J. Hydrogen Energy*, 2021, **46**, 27709–27730.
87 M. Naeini, H. Lai, J. S. Cotton and T. A. I. Adams, *Ind. Eng. Chem. Res.*, 2021, **60**, 1326–1340.
88 M. Z. Khan, A. Hussain, S.-B. Lee, T.-H. Lim and R.-H. Song, *Prog. Nat. Sci.:Mater. Int.*, 2024, **34**, 606–613.
89 M. H. Golbabaei, M. Saeidi Varnoosfaderani, A. Zare, H. Salari, F. Hemmati, H. Abdoli and B. Hamawandi, *Materials*, 2022, **15**, 7760.
90 V. Subotić, M. Eibl and C. Hochenauer, *Energy Convers. Manage.*, 2021, **230**, 113764.
91 G. Xu, Z. Yu, L. Xia, C. Wang and S. Ji, *Energy Convers. Manage.*, 2022, **268**, 116026.
92 W. W. Xing, A. A. Shah, G. Dai, Z. Zhang, T. Guo, H. Qiu, P. Leung, Q. Xu, X. Zhu and Q. Liao, *Int. J. Hydrogen Energy*, 2023, **48**, 23242–23257.
93 Z. Li, F. Liu, W. Yang, S. Peng and J. Zhou, *IEEE Trans. Neural Netw. Learn. Syst.*, 2022, **33**, 6999–7019.
94 A. Sciazko, Y. Komatsu, T. Shimura and N. Shikazono, *npj Comput. Mater.*, 2024, **10**, 1–15.
95 Z. Yan, A. He, S. Hara and N. Shikazono, *Energy Convers. Manage.*, 2019, **198**, 111916.
96 M. Raissi, P. Perdikaris and G. E. Karniadakis, *J. Comput. Phys.*, 2019, **378**, 686–707.
97 M. Berardi, F. V. Difonzo and M. Icardi, *Comput. Methods Appl. Mech. Eng.*, 2025, **435**, 117628.
98 R. Laubscher, *Phys. Fluids*, 2021, **33**, 087101.

